Supplementary Information

A General Bio-Inspired, Metals-Based Synergic Cross-Linking Strategy toward Mechanically Enhanced Materials

Ke Chen, Jin Ding, Shuhao Zhang, Xuke Tang, Yonghai Yue*, Lin Guo*

Experimental materials and methods

Materials. Graphite powder with particle size < 20 μm was used as received from Alfa Aesar, chitosan ($C_{6n}H_{11n}NO_{4n}$,CS) (Viscosity (*v*), > 400 mPa S) with molecular weight about 263.20 g mol^{-1}, polymethyl methacrylate (($C_5H_8O_2$)x, PMMA) (Polydispersity index (PDI), 1.57) with molecular weight about 534 Kg mol^{-1}, and glacial acetic acid were purchased from Aladdin industrial corporation (Shanghai, China). Sodium montmorillonite (Na-MTM) nanoclays were offered by Zhejiang Fengdong Clay Co Ltd. $MgCl_2 \cdot 6H_2O$ (99.0 - 102.0 %), $CuCl_2 \cdot 2H_2O$ (99.99 %), $Ni(NO_3)_2$ (99.99 %), $CaCl_2$ (99.9 %), $CoCl_2 \cdot 6H_2O$ (99.99 %), $TiOSO_4 \cdot XH_2SO_4 \cdot XH_2O$ (93.3 %), and $AlCl_3 \cdot 6H_2O$ (99.99 %) were purchased from Aladdin industrial corporation (Shanghai, China), and $ZrOCl_2 \cdot 8H_2O$ (99.9 %) was utilized as received from Alfa Aesar. All other reagents (*e.g.*, $KMnO_4$, H_2SO_4, NaOH, C_2H_5OH, and acetone, analytical grade) were used without further purification. Ultrapure doubly deionized water (Resistivity > 18.2 MΩ cm) in this work was obtained from a synergy UV water purification system (Millipore Corporation).

CN-CA filter membranes (0.22 μm pore size, 47 mm diameter) from Hai Cheng Shi Jie Filter Co. Ltd (Beijing, China) were used in filtration to support fabricated paper. Sonication was performed using a KQ-300VDE dual frequency ultrasonic cleaner from Kunshan Ultrasonic Instruments Co., Ltd (Jiangsu, China). A Sigma 2-16 centrifuge was employed for the centrifugation.

Methods. Preparation of graphene oxide (GO): GO was made following the modified Hummers method.[S1-S3] In a typical process, 3.0 g of natural graphite flakes (Alfa Aesar) was subjected to pre-oxidation treatment by stirring vigorously for 6 hrs at 80 °C in a mixture of $K_2S_2O_8$ (2.5 g), P_2O_5 (2.5 g), and H_2SO_4 (15 mL). The pre-oxidized graphite powder (about 3.5 g) was dried overnight before further oxidative treatment by stirring it in a mixture of 120 mL of H_2SO_4 and 15 g of $KMnO_4$ in an ice bath. Notably, $KMnO_4$ was slowly added with vigorous stirring to avoid the temperature rising above 20 °C. The solution was then transferred to 35 ± 3 °C water bath and stirred for about 1 hour before adding 250 mL of water. Add 700 mL of warm water and 20 mL of H_2O_2 (30 wt.%) to reduce $KMnO_4$ and MnO_2 to $MnSO_4$. The color of the blend solution turned to dark greenish yellow during the reduction. Then the warm solution was filtered. The GO slurry collected form membrane was then washed with 750 mL of 2 M HCl, and purified GO can be collected at the tube bottom after centrifugation, followed by centrifugation and careful washing with water to clean out remnant salt. The extracted GO was then re-dispersed in water (1 mg mL^{-1}) for vacuum filtration.

Preparation of the single/mixed M^{n+} ions solution: Firstly, diverse single M^{n+} solutions (0.05 mM) were successfully prepared in deionized water. Secondly, based on the molar ratio ($R_{Mg: Zr: Ni: Ca: Cu: Co: Ti: Al}$ = 137.5 : 274.0 : 1.8 : 82.5 : 3.2 : 0.1 : 5.0 : 851.0) of various minerals/elements in nacre (Figure S4a), including Mg, Ni, Ca, Cu, Co, and Al, the mixed $A^{2/3+}$ ions (Mg^{2+}, Ni^{2+}, Ca^{2+}, Cu^{2+}, Co^{2+} and Al^{3+}) aqueous solution were prepared, assuming the molar ratio of Mg^{2+} to Ca^{2+} was equal to 1: 1. And then ZrO^{2+} and TiO^{2+} ions aqueous solutions (0.05 mol L^{-1}) were prepared, respectively. Similarly, the mixed $A^{2/3+}$ ions, ZrO^{2+} (0.05 mol L^{-1}), and TiO^{2+} (0.05 mol L^{-1}) ions solutions were also prepared in acetone, respectively.

Preparation of Syn-M^{n+}-GO papers (SMGOs):

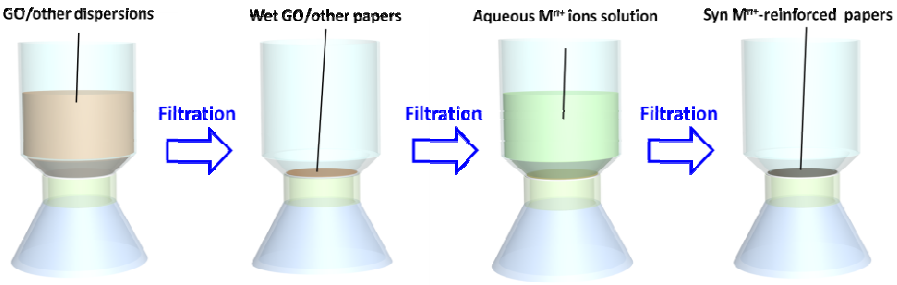

Figure S1 Schematic diagram for the preparation of the SMGOs through using the continuous vacuum filtration method.

Preparation of Syn-M^{n+}/CS (Syn-CS), Syn-M^{n+}/PMMA (Syn-PMMA), and Syn-M^{n+}/CS-MTM (Syn-CS/MTM) papers:

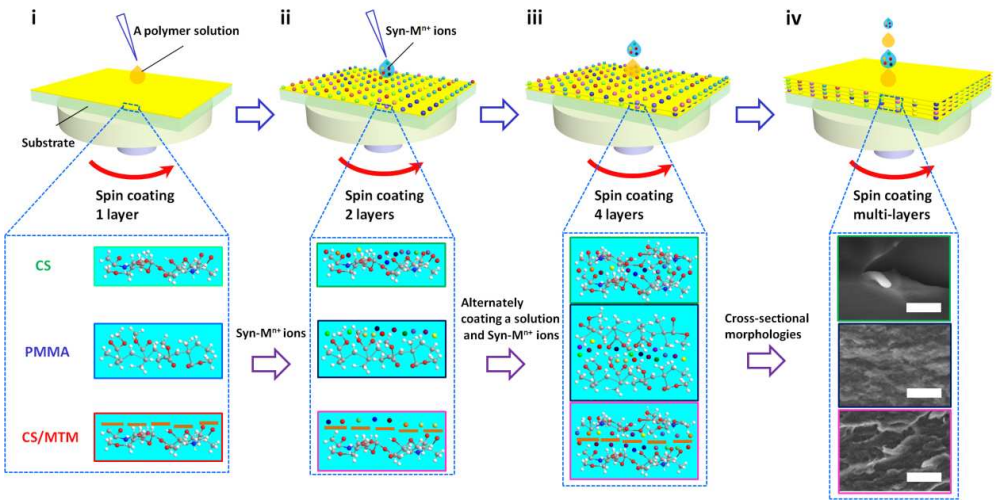

Figure S2 Bottom-up spin coating layer-by-layer (BSC-LBL) assembly, molecular models and cross-sectional morphologies of the nanocomposite films, such as Syn-CS, Syn-PMMA, and Syn-CS-MTM. (i-iv) The BSC-LBL assembly presents the multilayered formation process of these nanocomposite films; molecular models exhibit the interaction behaviours between various M^{n+} ions and these polymers by chemically synergic cross-linking bonding. Different color balls represent different M^{n+} ions and dark yellow bar stands for MTM nanosheets. Elements in the ball-and-stick model are color-coded: H: white, C: light grey, O: red, N: blue. Scale bar is 2.5 nm in scanning electron microscopy (SEM) images.

Preparation of pure GO and Syn-GO membranes:

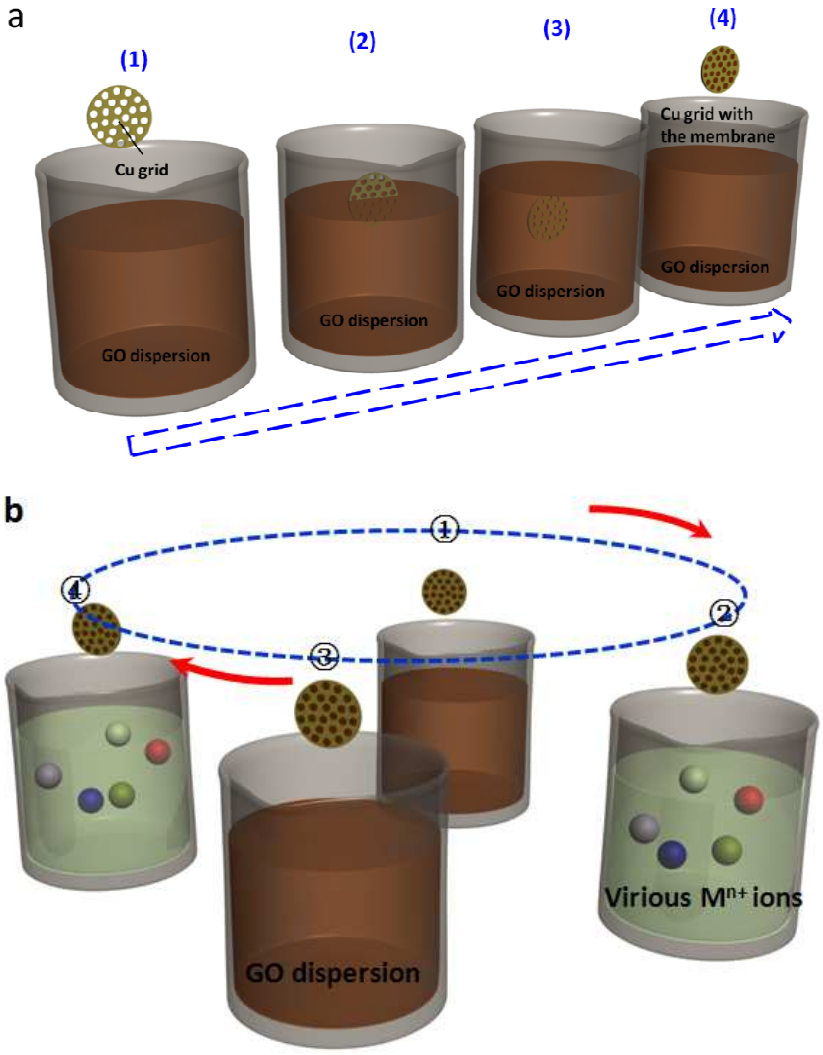

Figure S3 Schematic diagrams for fabrication of the pure GO and Syn-GO membranes by using the the layer-by-layer (LBL) assembly. (a) GO. (b) Syn-GO.

The 100-μm-diameter and 25-μm-thick micro copper grid substrate (Zhong Jing Ke Yi, Beijing) was used for GO growth under ambient condition (25 °C, 20 % RH)) for the suspended GO membranes. The colloidal GO dispersion (0.2 mg mL^{-1}) was utilized to assemble the suspended GO membranes (Figure S3a). Both colloidal GO dispersion and the mixed M^{n+} ion (5.0×1.0^{-4} mol L^{-1}) aqueous solutions were utilized to assemble the Syn-GO membranes (Figure S3b). To achieve a constant thickness of

these assembled membranes, the four assemblies were created by repeated dipping into the colloidal GO dispersion.

Nanodynamic mechanical Analysis (NanoDMA):

The damping behavior of visco−elastic materials is characterized by measuring the phase lag δ between the applied forced and the displacement response. A perfectly elastic material would have a phase lag of zero. The angle δ allows characterizing the moduli of a material as a complex modulus (E_c), followed in Eq. S1.

$$E_c = \frac{\sigma}{\varepsilon}(\cos\delta + i\sin\delta) \qquad \text{(S1)}$$

The moduli measured can thus be separated into two distinct moduli, the real part (E') and an imaginary part (E'') as shown in Eqs S2-S3.

$$E' = \frac{\sigma}{\varepsilon}(\cos\delta) \qquad \text{(S2)}$$

$$E'' = \frac{\sigma}{\varepsilon}(\sin\delta) \qquad \text{(S3)}$$

The real part is the storage modulus (E'), which represents the ability of the material to store potential energy and release it during deformation. The imaginary part is the loss modulus (E'') which represents the viscoelastic component responsible for the dissipated energy. Damping behavior is commonly quantified by the ratio of the loss modulus to the storage modulus which yield tan δ as displayed in Eq S4.

$$\frac{E''}{E'} = \frac{(\frac{\sigma}{\varepsilon}(\sin\delta))}{(\frac{\sigma}{\varepsilon}(\cos\delta))} = \tan\delta \qquad \text{(S4)}$$

Higher values of tan δ indicate a higher ratio of viscoelastic to elastic response in the material, thus tan δ serves as a measure of damping.

In this study, tan δ is evaluated at variable dynamic loads, varying quasi-static loading from 10 to 1200 μN which is divided by 50 segments, and constant frequency (50 Hz).

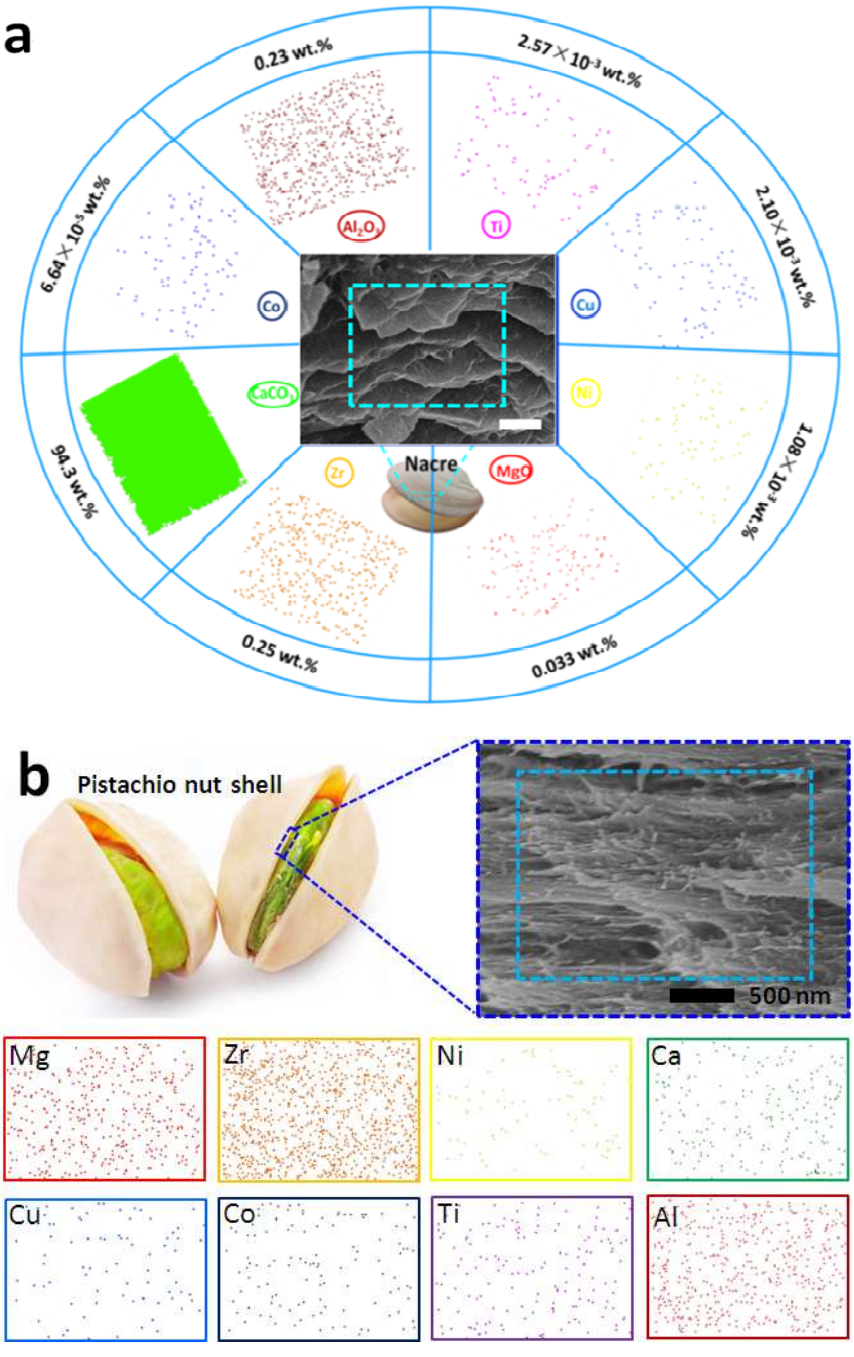

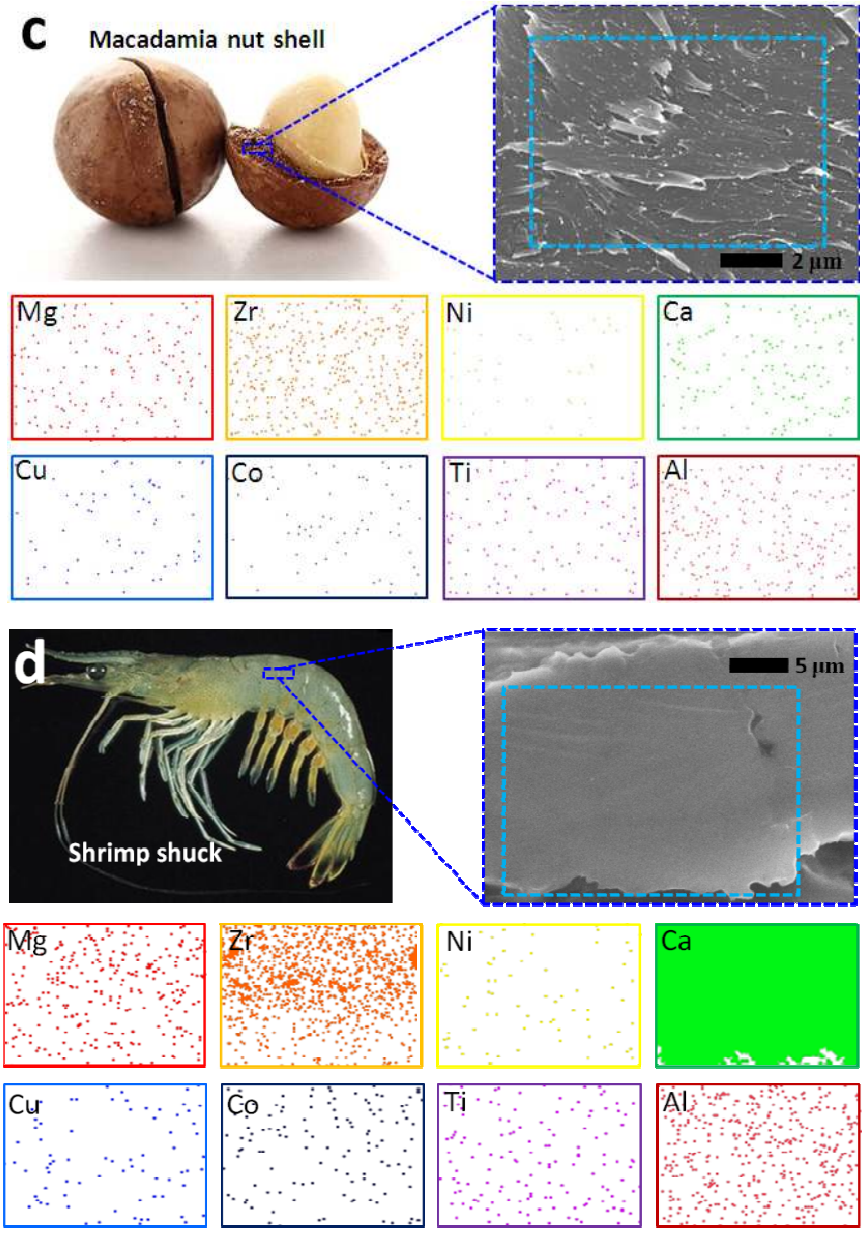
c
Macadamia nut shell
2 μm
Mg
Zr
Ni
Ca
Cu
Co
Ti
Al
d
Shrimp shuck
5 μm
Mg
Zr
Ni
Ca
Cu
Co
Ti
Al

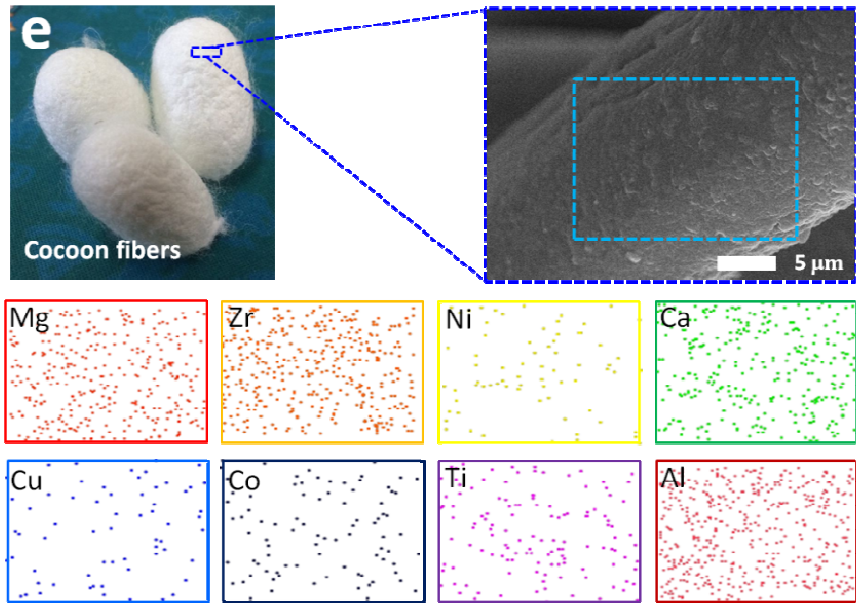

Figure S4 SEM-EDS element mappings of some natural materials, indicating the existence of various mineral elements in their structural constituents. (a) ICP-MS element analysis, together with element mappings of nacre from bivalve pearl oyster shell, indicating various elements/minerals (*e.g.*, Al, Ti, Cu, Zr, Co, Ni, and Mg) more than Ca. (b) *Pistachio* nut shell. (c) Macadamia shell. (d) Shrimp shucks. (e) Cocoon fibers.

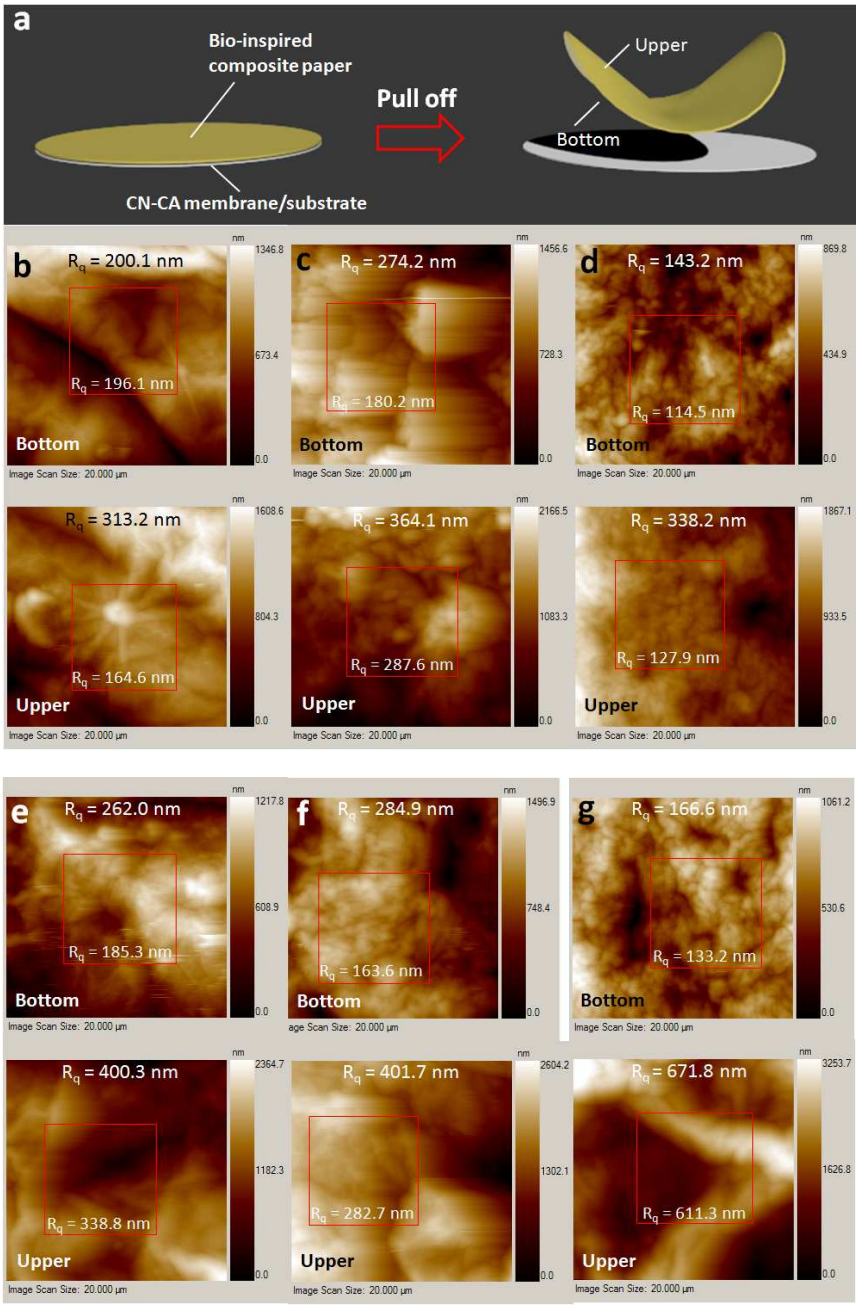
a
Bio-inspired composite paper
Pull off
Upper
Bottom
CN-CA membrane/substrate
b
R_q = 200.1 nm
R_q = 196.1 nm
Bottom
c
R_q = 274.2 nm
R_q = 180.2 nm
Bottom
d
R_q = 143.2 nm
R_q = 114.5 nm
Bottom
R_q = 313.2 nm
R_q = 164.6 nm
Upper
R_q = 364.1 nm
R_q = 287.6 nm
Upper
R_q = 338.2 nm
R_q = 127.9 nm
Upper
e
R_q = 262.0 nm
R_q = 185.3 nm
Bottom
f
R_q = 284.9 nm
R_q = 163.6 nm
Bottom
g
R_q = 166.6 nm
R_q = 133.2 nm
Bottom
R_q = 400.3 nm
R_q = 338.8 nm
Upper
R_q = 401.7 nm
R_q = 282.7 nm
Upper
R_q = 671.8 nm
R_q = 611.3 nm
Upper

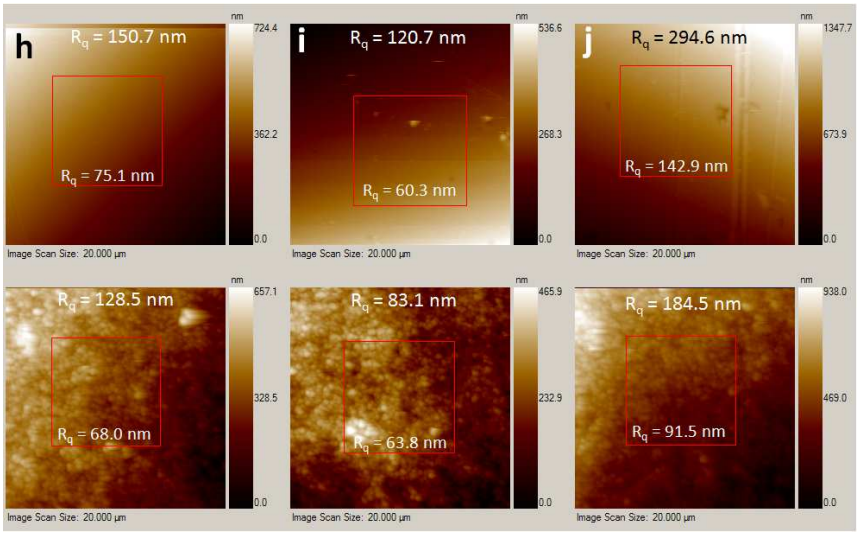

Figure S5 The root-mean square (RMS) roughness of these bio-inspired composite papers with upper and bottom surface within 20 µm × 20 µm and 10 µm × 10 µm areas (inside red boxes). (a) Schematic draws for showing the two sides (upper and bottom) of the paper, (b) GO, (c) A^{2+}-GO, (d) $A^{2/3+}$-GO, (e) $A^{2/3+}$-ZrO^{2+}-GO, (f) $A^{2/3+}$-TiO^{2+}-GO, (g) Syn-GO, (h) Syn-CS, (i) Syn-PMMA, (j) Syn-CS/MTM.

The typical RMS roughnesses of these composite papers were shown in Figure S5. In general, the RMS roughness (313.2 ~ 671.8 nm within a 20 µm × 20 µm area, 127.9 ~ 611.3 nm within a 10 µm × 10 µm area) at upper surface was higher than that (143.2 × 284.9 nm within a 20 µm × 20 µm area, 114.5 ~ 196.1 nm within a 10 µm × 10 µm area) at bottom surface for one of SMGOs, while the RMS roughness (83.1 ~ 184.5 nm within a 20 µm × 20 µm area, 63.8 ~ 91.5 nm within a 10 µm × 10 µm area) at upper surface was similar with that (120.7 ~ 294.6 nm within a 20 µm × 20 µm area, 60.3 ~ 142.9 nm within a 10 µm × 10 µm area) at bottom surface for one of them (Syn-CS, Syn-PMMA, or Syn-CS/MTM).

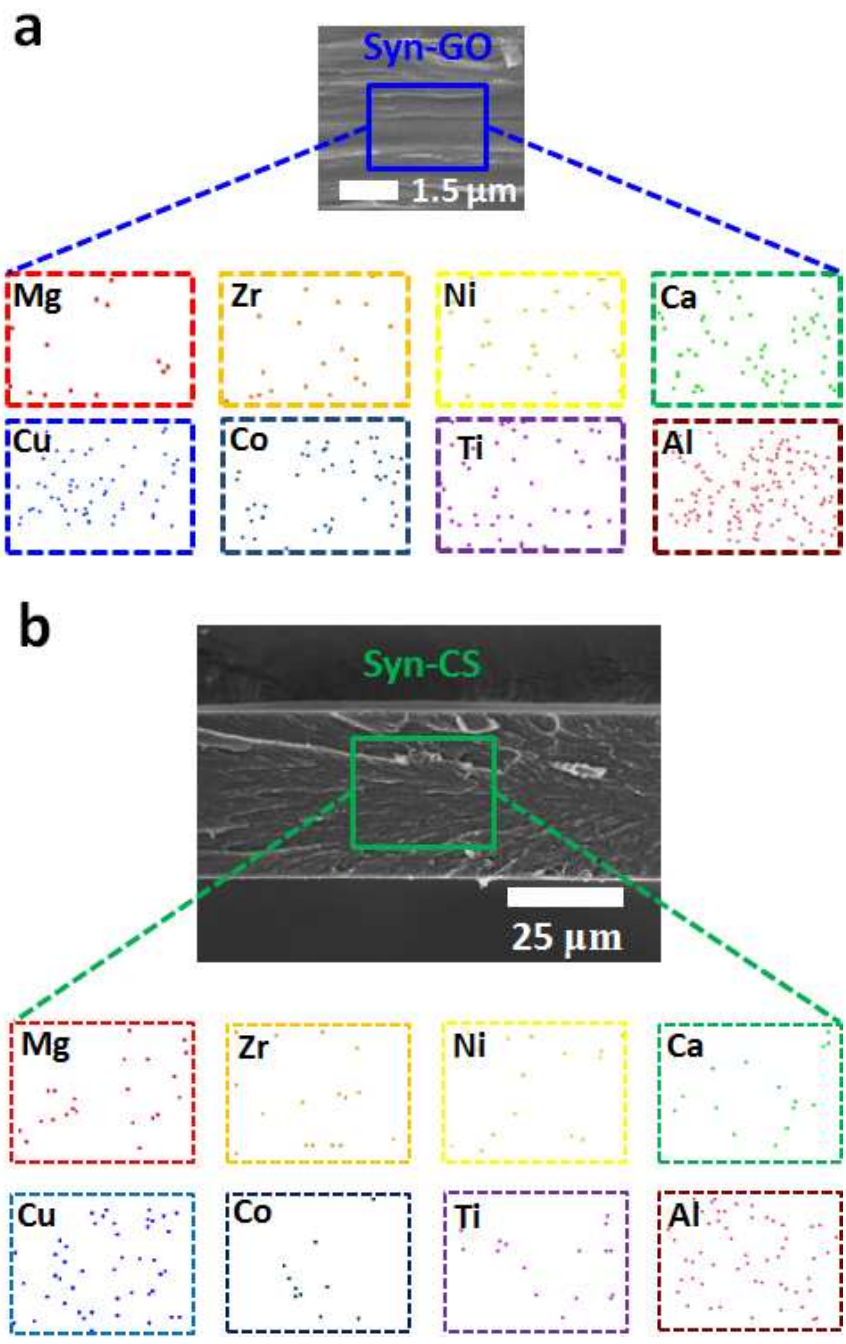
a
Syn-GO
1.5 µm
Mg
Zr
Ni
Ca
Cu
Co
Ti
Al
b
Syn-CS
25 µm
Mg
Zr
Ni
Ca
Cu
Co
Ti
Al

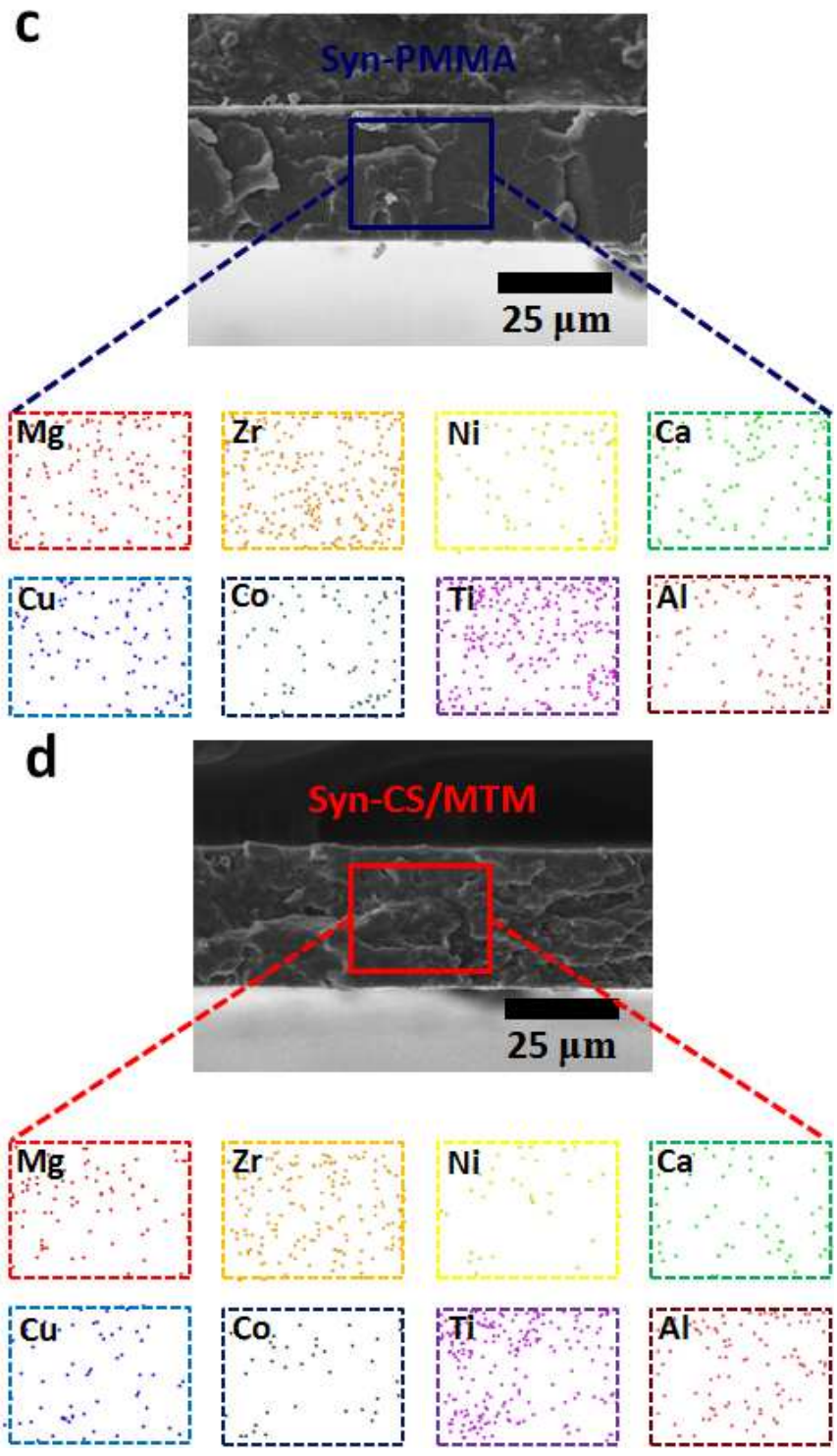

Figure S6 SEM-EDS element mappings of the cross-section images for these bio-inspired composites. (a) Syn-GO. (b) Syn-CS. (c) Syn-PMMA. (d) Syn-CS/MTM.

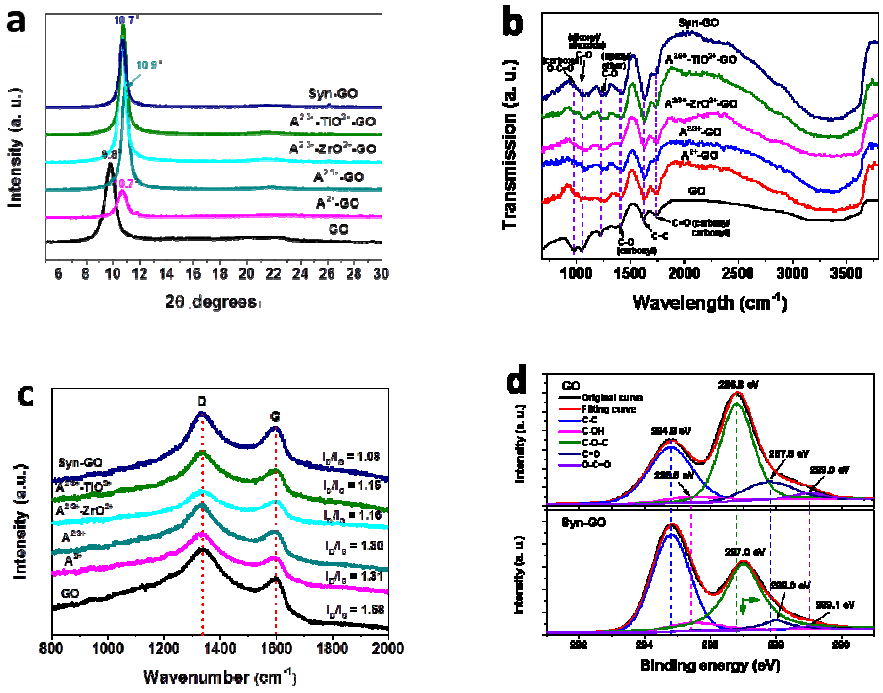

Figure S7 Characterization of SMGO papers. (a) X-ray diffraction (XRD) patterns. (b) Fourier transform infrared (FTIR). (c) Raman spectra. (d) The deconvoluted X-ray photoelectron spectroscopy (XPS) in the C 1s region.

XRD was used to study the change of the intercalation of M^{n+} ions in the gallery spacing (*d*-spacing) of GO nanosheets (Figure S7a). The *d*-spacing of pure GO is about 9.0 Å ($2\theta = 9.8°$).

Table S1 Summary of macro-micromechancial properties for metal ion-cross-linked composite papers.

Materials	Adding ions content (μL)	σ (MPa)	W (MJ m^{-3})	E (GPa)	E' (GPa)	H (GPa)
GO	-	87.9 ± 14.4	2.4 ± 1.5	4.5 ± 0.2	1.8 ± 0.1	0.17 ± 0.08
A^{2+}	60	125 ± 15.5	1.5 ± 0.3	7.9 ± 1.0	2.4 ± 0.2	0.33 ± 0.04
$A^{2/3+}$	40	120 ± 9.6	1.0 ± 0.1	7.6 ± 1.1	1.9 ± 0.1	0.24 ± 0.02

$A^{2/3+}$-ZrO^{2+}	60	130 ± 15.5	1.6 ± 0.1	5.1 ± 2.1	2.0 ± 0.3	0.21 ± 0.01
$A^{2/3+}$-TiO^{2+}	40	150.4 ± 2.1	1.7 ± 0.2	7.2 ± 1.9	3.0 ± 0.1	0.33 ± 0.02
Syn-GO	40	150.2 ± 12.2	2.0 ± 0.2	7.5 ± 1.4	5.1 ± 1.0	0.47 ± 0.10
Mg^{2+}	20	116.3 ± 5.4	2.3 ± 0.2	7.2 ± 1.2	2.6 ± 0.5	0.32 ± 0.04
ZrO^{2+}	40	87.2 ± 7.0	0.7 ± 0.1	7.4 ± 0.3	3.0 ± 0.7	0.26 ± 0.06
Ni^{2+}-GO	20	137.5 ± 12.2	2.1 ± 0.5	12.4 ± 0.9	4.8 ± 0.4	0.38 ± 0.06
Ca^{2+}-GO	80	116.7 ± 8.3	1.4 ± 0.3	9.1 ± 0.4	4.2 ± 0.7	0.58 ± 0.09
Cu^{2+}-GO	60	86.8 ± 5.4	4.6 ± 0.7	2.8 ± 0.3	2.3 ± 0.6	0.24 ± 0.1
Co^{2+}-GO	20	98.8 ± 6.4	1.0 ± 0.3	6.1 ± 0.4	3.9 ± 0.8	0.31 ± 0.07
TiO^{2+}-GO	20	132.5 ± 6.1	2.5 ± 0.6	6.6 ± 0.9	2.5 ± 0.8	0.25 ± 0.07
Al^{3+}-GO	40	117.3 ± 6.5	1.2 ± 0.1	8.4 ± 1.1	4.2 ± 0.8	0.40 ± 0.04
Syn-CS		132.4 ± 19.7	38.9 ± 9.2	3.0 ± 0.2	5.3 ± 0.3	0.33 ± 0.04
PMMA		34.3 ± 3.1	0.6 ± 0.3	1.3 ± 0.4	3.7 ± 0.1	0.23 ± 0.06
Syn-PMMA		61.0 ± 9.5	5.0 ± 2.8	1.8 ± 0.3	4.6 ± 0.2	0.27 ± 0.01
CS/MTM		137.2 ± 17.4	19.8 ± 4.8	3.7 ± 0.5	5.0 ± 0.2	0.32 ± 0.04
Syn-CS/MTM		193.2 ± 17.3	41.6 ± 3.4	4.5 ± 1.0	7.1 ± 0.5	0.36 ± 0.06

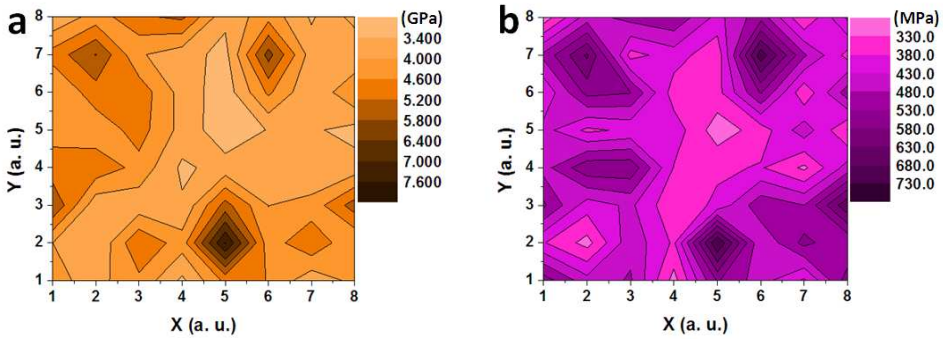

Figure S8 The contour maps of E'_g (a) and H'_g (b) dispersion on the Syn-GO paper plane within a 20 μm × 20 μm area (P'_{max} = 1000 μN).

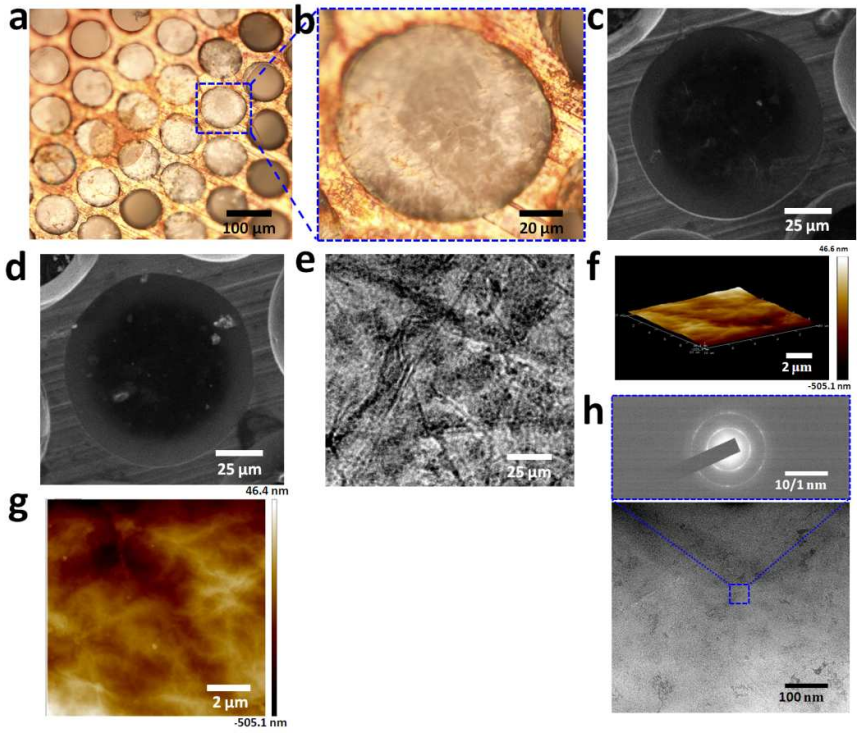

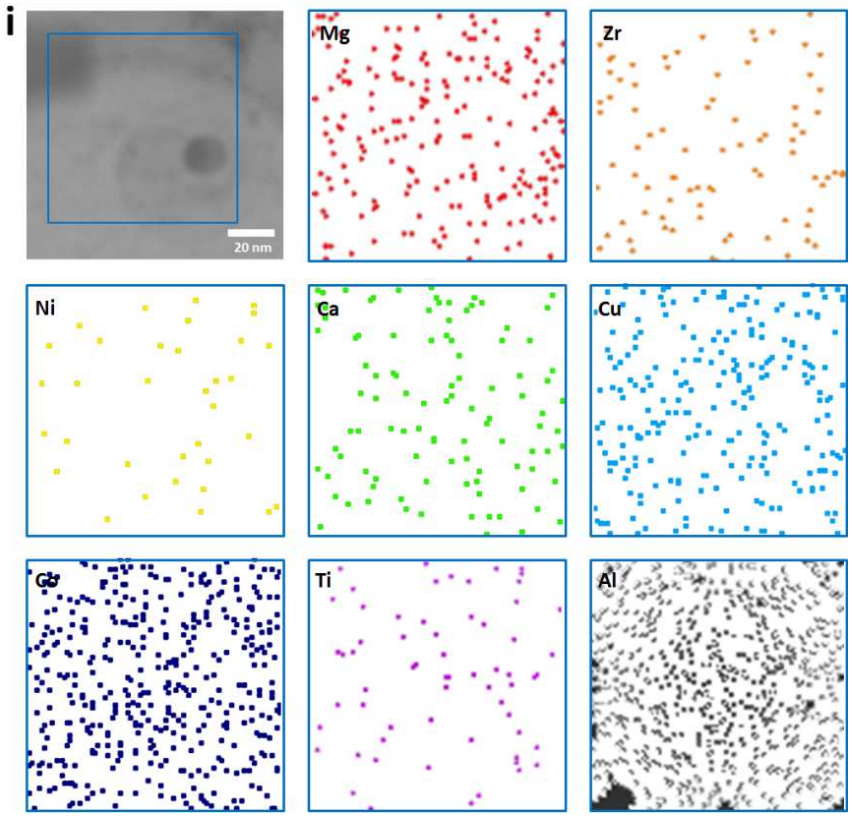

Figure S9 Characterization of the Syn-GO membrane over the holes of a copper grid. (a-b) Optical micrograph of the suspended membranes (a) and one magnifying membrane (b) in a. (c-e) SEM images of the random suspended membranes, indicating the structural feature of the membrane with some wrinkles. (f-h) AFM (f and g) and TEM images (h) with SAED pattern of the suspended partial membranes with a RMS roughness of 54.0 nm within a 10.0 μm ×10.0 μm area, indicating the assembled membranes originated from the multilayered stacking faults of the GO sheets. (i) EDS-element mapping analysis over hole of a molybdenum grid.

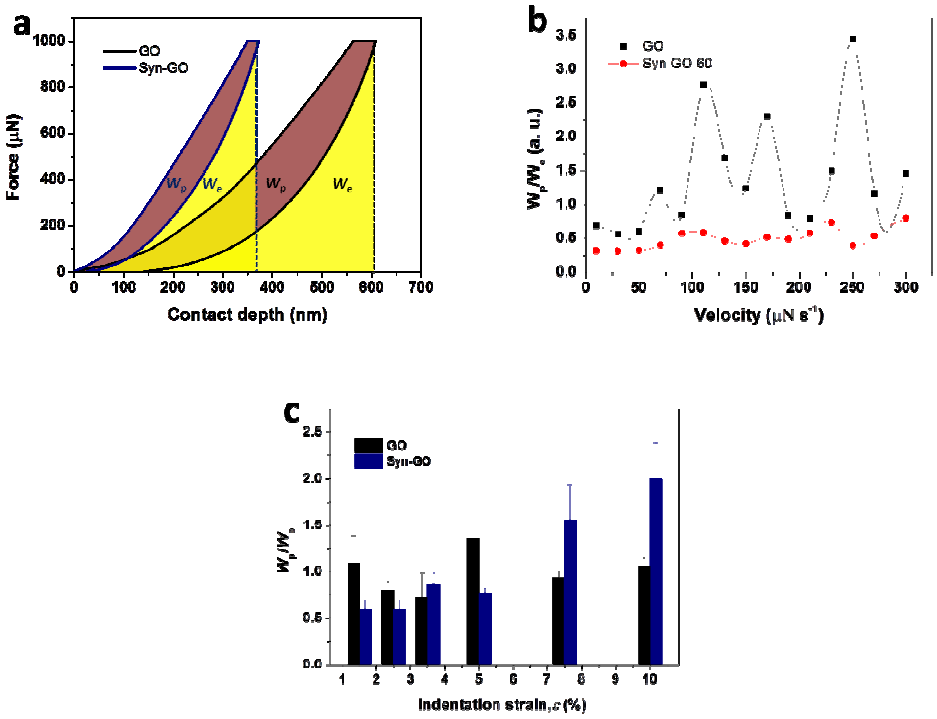

Figure S10 Comparison of energy absorption by plastic and elastic deformations for GO and Syn-GO during a contact cycle. (a) Definition of the elastic energy (W_e), the plastic energy (W_p), and total contact energy (W_t) based on the displacement control indentation on the cross-section of the sample. (b) (W_p/W_e) dependent on loading velocity from 10 to 300 μN S^{-1} during loading of 200 μN. (c) W_p/W_e dependent on indentation strain during a contact cycles.

Table S2 Summary of the mechanical improvement of the samples with M^{n+} ions in comparison with those samples without any M^{n+} ions.

Materials	% (σ)	% (W)	% (E)	% (E')	% (H)
GO	0	0	0	0	0
A^{2+}-GO	~42.2	~-37.5	~75.6	~33.3	~94.1
$A^{2/3+}$-GO	~36.5	~-58.3	~68.9	~5.6	~41.1
$A^{2/3+}$-ZrO^{2+}-GO	~47.9	~-33.3	~13.3	~11.1	~23.5

$A^{2/3+}$-TiO^{2+}-GO	~71.1	~-29.2	~60	~66.7	~94.1
Syn-GO	~70.8	~-16.7	~66.7	~183.3	~176.5
CS; PMMA; CS-MTM	0	0	0	0	0
Syn/CS	~24.1	~18.6	~25.0	~8.2	~6.4
Syn/PMMA	~77.8	~733.3	~38.5	~24.3	~12.5
Syn-CS/MTM	~40.8	~110.1	~21.6	~42.0	~12.5

Table S3 Summary of mechanical properties for metal ion-related films/papers and other related materials.

Samples	σ (MPa)	W (MJ m^{-3})	E (GPa)	Samples	σ (MPa)	W (MJ m^{-3})	E (GPa)	Publication Years
GO	~89.7	~0.43	~7.6	**Al^{3+}-GO**	~120	~0.27	~26.2	2015[S4]
GO	~77.7	~0.64	~8.0	**Fe^{3+}-GO**	~92.5	~0.47	~9.6	2015[S5]
GO/TA	~68.3	~0.46	~8.9	**Fe^{3+}-GO/TA**	~169.3	~0.35	~49.7	2015[S5]
MTM/CMC[1]	~160	~2.6	~11.7	**Cu^{2+}-MTM/CMC[1]**	~195	~1.7	~21.3	2013[S6]
MTM/CMC[2]	~175	~5.3	~11.2	**Cu^{2+}-MTM/CMC[2]**	~240	~2.1	~20.5	2013[S6]
GO	~81.9	~25.6	~0.16	**Mg^{2+}-GO**	~80.6	~0.18	~27.9	2008[S7]
				Ca^{2+}-GO	~125.8	~0.31	~28.1	2008[S7]
MTM/PDDA	-	-	-	**Ca^{2+}-MTM/PDDA**	~109	~0.96	~13.0	2003[S8]
PVA	~43.0	~10.4	~0.43	**PVA/MTM**	~110	~0.43	~14.1	2007[S9]
				GA-MTM/PVA	~400	~0.68	~106.0	
CS	~50	~16.6	~0.14	**Al_2O_3/CS**	~315	~69.9	~9.6	2008[S10]
PMMA	~12.2	~0.42	~0.67	**GO/PMMA**	~148.3	~2.4	~7.5	2010[S11]
UFOs	-	-	-	**UFOs/MTM**	~140	~7.5	~3.8	2011[S12]
PMMA	~62.0	~1.8	~12.0	**GO/PMMA**	~76.0	~1.0	~2.7	2012[S13]
CMC	~151	~12.3	~5.8	**CMC/MTM**	~320	~4.0	~25.0	2013[S14]
GO	~106.3	~1.7	~3.8	**GO/CS**	~346.1	~6.6	~19.0	2015[S15]
CS	~107.3	~30.9	~0.27					

*Abbreviations: PDDA, poly (diallyldimethylammonium chloride); PVA, poly (vinyl alcohol); GA, glutaraldehyde; UFOs, urea-formaldehyde oligomers.

References

(S1) Hummers, W. S.; Offeman, R. E. Preparation of Graphitic Oxide. *J. Am. Chem. Soc.* **1958**, *80*, 1339-1339.

(S2) Compton, O. C.; Cranford, S. W.; Putz, K. W.; An, Z.; Brinson, L. C.; Buehler, M. J.; Nguyen, S. T. Tuning the Mechanical Properties of Graphene Oxide Paper and Its Associated Polymer Nanocomposites by Controlling Cooperative Intersheet Hydrogen Bonding. *ACS Nano* **2012**, *6*, 2008-2019.

(S3) Dimiev, A.; Kosynkin, D. V.; Alemany, L. B.; Chaguine, P.; Tour, J. M. Pristine Graphite Oxide. *J. Am. Chem. Soc.* **2012**, *134*, 2815-2822.

(S4) Yeh, C.-N.; Raidongia, K.; Shao, J.; Yang, Q.-H.; Huang, J. On the Origin of the Stability of Graphene Oxide Membrane in Water. *Nat. Chem.* **2015**, *7*, 166-170.

(S5) Liu, R. Y.; Xu, A. W. Byssal Threads Inspired Ionic Cross-Linked Narce-Like Graphene Oxide Paper with Superior Mechanical Strength. *RSC Adv.* **2014**, *4,*40390-40395.

(S6) Das, P.; Walther, A. Ionic Supramolecular Bonds Preserve Mechanical Properties and Enable Synergetic Performance at High Humidity in Water-Borne, Self-Assembled Nacre-Mimetics. *Nanoscale* **2013**, *5*, 9348-9356.

(S7) Park, S.; Lee, K. S.; Bozoklu, G.; Cai, W.; Nguyen, S. T.; Ruoff, R. S. Graphene Oxide Papers Modified by Divalent Ions-Enhancing Mechanical Properties *via* Chemical Cross-Linking. *ACS Nano* **2008**, *2*, 572-578.

(S8) Tang, Z.; Kotov, N. A.; Magonov, S.; Ozturk, B. Nanostructured Artificial Nacre. *Nat. Mater.* **2003**, *2*, 413-418.

(S9) Podsiadlo, P.; Kaushik, A. K.; Arruda, E. M.; Waas, A. M.; Shim, B. S.; Xu, J. Nandivada, H.; Pumplin, B. G.; Lahann, J.; Ramamoorthy, A.; Kotov, N. A. Ultrastrong and Stiff Layered Polymer Nanocomposites. *Science* **2007**, *318*, 80-83.

(S10) Bonderer, L. J.; Studart, A. R.; Gauckler, L. J. Bioinspired Design and Assembly of Platelet Reinforced Polymer Films. *Science* **2008**, *319*, 1069-1073.

(S11) Putz, K. W.; Compton, O. C.; Palmeri, M. J.; Nguyen, S. T.; Brinson, L. C. High-Nanofiller-Content Graphene Oxide-Polymer Nanocomposites *via* Vacuum-Assisted Self-Assembly. *Adv. Funct. Mater.* **2010**, *20*, 3322-3329.

(S12) Inagamov, S. Y.; Mukhamedov, G. I. Structure and Physical-Mechanical Properties of Interpolymeric Complexes Based on Sodium Carboxymethylcellulose. *J. Appl. Polym. Sci.* **2011**, *122*, 1749-1757.

(S13) Morimune, S.; Nishino, T.; Goto, T. Ecological Approach to Graphene Oxide Reinforced Poly (Methyl Methacrylate) Nanocomposites. *ACS Appl. Mater. Interfaces* **2012**, *4*, 3596-3601.

(S14) Das, P.; Schipmann, S.; Malho, J. M.; Zhu, B.; Klemradt, U.; Walther, A. Facile Access to Large-Scale, Self-Assembled, Nacre-Inspired, High-Performance Materials with Tunable Nanoscale Periodicities. *ACS Appl. Mater. Interfaces* **2013**, *5*, 3738-3747.

(S15) Wan, S.; Peng, J.; Li, Y.; Hu, H.; Jiang, L.; Cheng, Q. Use of Synergistic Interactions to Fabricate Strong, Tough, and Conductive Artificial Nacre Based on Graphene Oxide and Chitosan. *ACS Nano* **2015**, *9*, 9830-9836.